

# AUTONOMOUS NODE SELECTION FOR WIRELESS NETWORKS OF BEARINGS-ONLY SENSORS\*

Lance M. Kaplan  
Dept. of Engineering  
Center for Theoretical Studies of Physical Systems  
Clark Atlanta University  
Atlanta, GA 30314

Peter Molnar  
Dept. of Comp. Sci.

Nino Srour    Andree Filipov  
U.S. Army Research Laboratory  
2800 Powder Mill Road  
Adelphi, MD 20783

## ABSTRACT

This paper introduces a decentralized node selection algorithm, which we name *autonomous node selection* (ANS). The purpose of a node selection algorithm is to select the active nodes that sense, compute and communicate measurements for target tracking in a wireless sensor network. By selecting a small number of active nodes, the sensor network will be functional over a longer lifetime. At each node, the ANS uses information about the local node and the active nodes to determine whether or not to be active for the next snapshot. In contrast, global approaches require information about all nodes in the network. We compare the ANS with global node selection algorithms by integrating them in an EKF tracker. Simulation results show that the ANS is comparable to global selection algorithms while exploiting only local information.

## 1 INTRODUCTION

Wireless networks of unattended ground sensors promise to provide revolutionary surveillance capabilities for the Objective Force. Such networks will be comprised of low cost nodes that can be easily deployable by cannon fire, artillery fire, airdrop, or hand emplacement. By communicating through their RF links, the nodes will form an autonomous, self-healing network that acts as a versatile large multi-node, multi-modality array for target detection, classification and tracking. To minimize bandwidth requirements and maximize operational life, the nodes will perform target analysis and data fusion in a decentralized manner. As a result, the performance of the sensor network will degrade gracefully if nodes fail. For the networks to be sustainable, intelligent node management is necessary so that power is conserved. A node manager determines the state of nodes by responding to targets detected in the scene and the operational requirements of the application for tracking

and classifying the targets. Activation of only those nodes that provide the best views of the target for localization and identification will result in significant power conservation. This paper will present our current work to develop an autonomous node manager. In order to reduce bandwidth/power requirements and improve information confidence, the node manager is distributed over all nodes; and each node independently determines its function given the information about the scene it has acquired from neighboring nodes in the network.

At the present time, we are investigating a network of bearing-only sensors with each node containing a circular array of microphones. The nodes can estimate the direction of arrival (DOA) of target sources using the acoustical array. By combining DOA estimates at a single snapshot, the network can localize the position of the targets. An extended Kalman filter can track the target over multiple snapshots. In this paper, we present an autonomous algorithm to be used by each node to determine whether or not it should estimate and communicate a DOA to other nodes. This algorithm determines which subset of nodes in the network can provide a good geometry to localize the target based on the predicted target position determined by the tracker.

This paper is organized as follows. Section 2 details the bearing measurement model and Section 3 discusses single snapshot localization and multiple snapshot tracking. The effect of node/target geometry on localization accuracy is analyzed in Section 4. Section 5 describes two global node selection approaches, and Section 6 introduces the decentralized autonomous node selection algorithm. Simulation results are provided in Section 7. Finally, Section 8 concludes the paper.

## 2 MEASUREMENT MODEL

To understand the behavior of a notional system consisting of tens to hundreds of acoustical nodes, we simulate and evaluate such systems using an additive white Gaussian noise (AWGN) measurement model. For the  $i$ -th node, the

---

\*Prepared through collaborative participation in the Advanced Sensors Collaborative Technology Alliance sponsored by the U.S. Army Research Laboratory under Cooperative Agreement DAAD19-01-2-008.

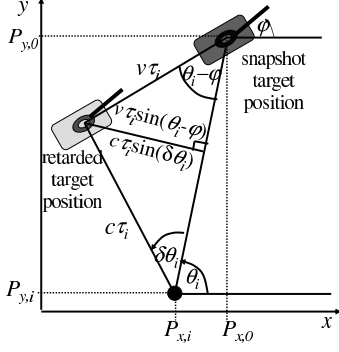


Figure 1: Illustration of the relationship between the snapshot DOA and retarded DOA for the  $i$ -th sensor.

measured DOA is related to the true DOA via

$$\hat{\theta}_i = \theta_i + \eta_i, \quad (1)$$

where  $\eta_i \sim N(0, \sigma_i^2)$ . We assume the nodes are sufficiently spaced so that  $\eta_i$  are independent between nodes and measurement intervals, i.e., snapshot times. If the target is stationary, the true DOA  $\theta_i$  is a function of the position of the  $i$ -th node relative to the target. Given that the **absolute** 2-D position of the  $i$ -th node in Cartesian coordinates is  $\vec{p}_i = (p_{x,i}, p_{y,i})$ , then the true DOA for a stationary target is

$$\tilde{\theta}_i = \arctan\left(\frac{p_{y,0} - p_{y,i}}{p_{x,0} - p_{x,i}}\right), \quad (2)$$

where  $\vec{p}_0$  is the target position. However, when the target is moving, the true DOA points to the target at a retarded position when it generated the acoustic energy measured at the snapshot time. The retarded position can differ from the snapshot position due to the propagation delay of the acoustic energy. Figure 1 shows that when a target moves at a constant velocity, the true DOA at the  $i$ -th node is function of both the relative location of the node and the velocity of the target via

$$\theta_i = \tilde{\theta}_i + \arcsin\left(\frac{v}{c} \sin(\tilde{\theta}_i - \psi)\right), \quad (3)$$

where  $c$  is the speed of sound,  $v$  is the target speed and  $\psi$  is the target heading. For this paper, we assume that  $c = 347\text{m/s}$ . In our simulations, we use (1)-(3) to generate bearing measurements.

The measurement model requires values for the bearing measurement error  $\sigma_i$  at each node. This error is a function of the signal to noise ratio (SNR) at the node. Clearly, the strength of the acoustic target signal impinging on the node depends on the propagation loss between the target and the node. The target signal strength is a complicated function of 1) the locations of the sensor and the target and 2) the meteorological conditions. Models do exist that can predict propagation loss under different weather conditions,

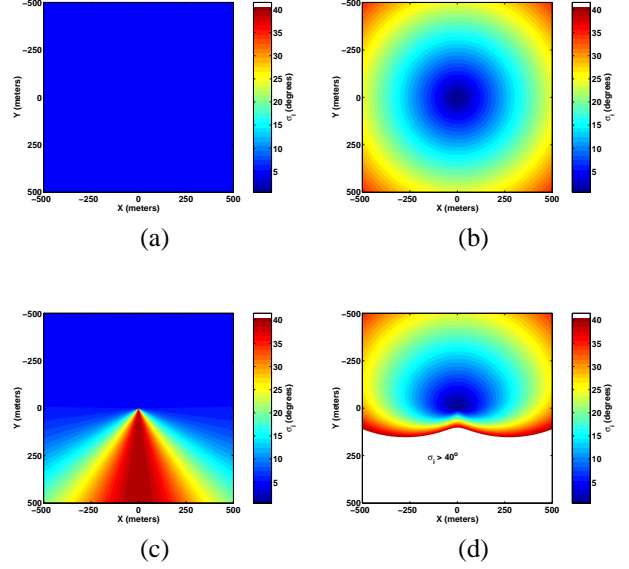


Figure 2: Bearing error  $\sigma_i$  in degrees as a function of relative position from the target for various models: (a) Isotropic with  $\alpha = 0$ , (b) isotropic with  $\alpha = 1$ , (c) anisotropic with  $\alpha = 0$  and (d) anisotropic with  $\alpha = 1$ .

e.g., (Magill and Swanson 1999). In practice, the implementations of such models will require meteorological sensors communicating with the UGS network. The determination of the SNR is further complicated by the multitude of sources of interfering noise sources. To make the analysis of target localization techniques tractable, we consider the following model for the bearing error,

$$\sigma_i = r_i^\alpha f(\phi_i) \quad (4)$$

where  $r_i$  and  $\phi_i$  are the 2-D polar coordinates for the position of the  $i$ -th node **relative** to the target. The function  $f(\cdot)$  allows for an anisotropic model in order to consider the case when the wind is blowing in a given direction. When  $f(\cdot)$  is constant, i.e.,  $f(\cdot) = k$ , the bearing error model is isotropic. The exponent  $\alpha$  controls degree of signal loss as a function of range to the target. When  $\alpha = 0$ , the bearing errors do not depend on range, and when  $\alpha > 0$ , the bearing errors increase with range. Figure 2 illustrates the relationship between the bearing error models used in our simulations. In the figure, the target is located at the center and the bearing errors are normalized to a value of  $5^\circ$  at a range of 100m in the most favorable direction.

### 3 TARGET MOTION ANALYSIS

#### 3.1 Localization

Using DOA measurements collected at a single snapshot, it is possible to estimate the state of the target, i.e., position and velocity. In (Kaplan et al. 2001a,b; Kaplan and Le

2002), we analyzed the performance of many different localization techniques. These techniques fall into two main categories. The first class of techniques assume the target is stationary so that the DOA measurement model is given by (1) and (2) where  $\tilde{\theta}_i = \theta_i$ . These methods, which we refer to as *two state* (TS) techniques, use the DOA measurements to estimate the 2-D position of the target. In this paper, we initialize tracking using the two state weighted least squares (TS-WNLS) technique:

$$\hat{p}_0 = \arg \min_{\vec{p}_0} \sum_{i=1}^{N_s} \frac{1}{\sigma_i^2} |\tilde{\theta}_i(\vec{p}_0) - \hat{\theta}_i|^2. \quad (5)$$

The TS-WNLS method is equivalent to the classical localization methods considered in (Kadar 1998; Nardone et al. 1984). It assumes that the bearing error  $\sigma_i$  is known for each node. There exists direction finding algorithms that can jointly estimate the DOA and SNR of a source signal (Bethel and Bell 2002). In turn, the estimate of the SNR can be used to estimate  $\sigma_i$ .

The second class of algorithms assumes the target is moving at a constant velocity by using (1)-(3) to estimate the 2-D position and velocity of the target. We refer to these methods as *four state* (FS) techniques. In our previous work, we showed that unlike the TS techniques, the FS methods provide unbiased position estimates for constant velocity targets. However, the variance of the position estimates is larger for the FS methods because they must estimate twice as many parameters than the TS methods. For small bearing errors  $\sigma_i$ , the FS methods are superior because they are unbiased. When the bearing errors exceed a few degrees, the variance of the FS methods become large enough so that the TS methods provide better position estimates. Therefore, we believe that the TS methods should be implemented in practice, and we only consider exploiting single snapshot data to extract the position estimates.

The focus of the node selection techniques is to select the active set of nodes  $\mathcal{N}_a$  of fixed cardinality  $|\mathcal{N}_a| = N_a$  that minimizes the root mean squared (RMS) position error when implementing TS localization. This RMS error is a function of the location of the nodes relative to the target. By ignoring the bias, the RMS position error can be computed from the covariance of the position error by (Kadar 1998; Kaplan 2002)

$$\rho = \sqrt{\text{trace} \{ \mathbf{J}^{-1} \}}, \quad (6)$$

where  $\mathbf{J}$  is the Fisher information matrix, i.e., the inverse the position covariance such that

$$\mathbf{J} = \sum_{i \in \mathcal{N}_a} \frac{1}{\sigma_i^2} \frac{1}{r_i^2} \begin{pmatrix} \sin^2 \phi_i & -\sin \phi_i \cos \phi_i \\ -\sin \phi_i \cos \phi_i & \cos^2 \phi_i \end{pmatrix}. \quad (7)$$

For this paper, we chose to ignore the bias because it adds an extra degree of complexity to the node selection process. We plan to consider estimates of the bias developed

in (Kaplan and Le 2002) to improve node selection in future work.

### 3.2 Tracking

We use a four state decentralized extended Kalman filter (EKF) to aggregate DOA measurements from the multiple snapshots. The decentralized EKF is a modification of the bearings-only EKF (Peach 1995) and the decentralized Kalman filter (Rao and Durrant-Whyte 1991). The dynamical model relates the target states  $\vec{x}$ , i.e., position and velocity, at the  $k+1$  and  $k$  snapshots via

$$\vec{x}(k+1) = \mathbf{F}\vec{x}(k) + \mathbf{A}\vec{v}(k+1),$$

where

$$\mathbf{F} = \begin{bmatrix} 1 & 0 & T & 0 \\ 0 & 1 & 0 & T \\ 0 & 0 & 1 & 0 \\ 0 & 0 & 0 & 1 \end{bmatrix}, \quad \mathbf{A} = \begin{bmatrix} 0.5T^2 & 0 \\ 0 & 0.5T^2 \\ T & 0 \\ 0 & T \end{bmatrix},$$

$T$  is the time between snapshots, and  $\vec{v}(k+1) \sim N(\vec{0}, \sigma_\nu^2 \mathbf{I})$  represents the acceleration of the target as a statistical perturbation. The value of  $\sigma_\nu$  controls the tradeoff between tracking convergence for a constant velocity target and the flexibility to track a maneuvering, e.g., accelerating, target. The measurement equation assumes a stationary target through augmentation of (1) and (2) over the set of active sensors  $\mathcal{N}_a$  for snapshot  $k+1$ ,

$$\vec{z}(k+1) = H(\vec{x}(k+1)) + \vec{\eta}(k+1),$$

where  $\vec{z} = [\hat{\theta}_{i_1}, \hat{\theta}_{i_2}, \dots, \hat{\theta}_{i_{N_a}}]^T$ ,  $\vec{\eta}(k+1) = [\eta_{i_1}, \eta_{i_2}, \dots, \eta_{i_{N_a}}]^T$  and

$$H(\vec{x}) = \begin{bmatrix} H_{i_1}(\vec{x}) \\ H_{i_2}(\vec{x}) \\ \vdots \\ H_{i_{N_a}}(\vec{x}) \end{bmatrix} = \begin{bmatrix} \arctan \left( \frac{x_2 - p_{y, i_1}}{x_1 - p_{x, i_1}} \right) \\ \arctan \left( \frac{x_2 - p_{y, i_2}}{x_1 - p_{x, i_2}} \right) \\ \vdots \\ \arctan \left( \frac{x_2 - p_{y, i_{N_a}}}{x_1 - p_{x, i_{N_a}}} \right) \end{bmatrix}.$$

Note that the measurement noise vector  $\vec{\eta}(k+1)$  is zero mean with a diagonal covariance matrix  $\mathbf{R}(k+1) = \text{diag}\{\sigma_{i_1}^2, \sigma_{i_2}^2, \dots, \sigma_{i_{N_a}}^2\}$ . Algorithms to select the active set of nodes are described in Sections 5 and 6.

The prediction equations for the EKF are given by

$$\hat{\vec{x}}(k+1|k) = \mathbf{F}\hat{\vec{x}}(k|k), \quad (8)$$

$$\mathbf{P}(k+1|k) = \mathbf{F}\mathbf{P}(k|k)\mathbf{F}^T + \sigma_\nu^2 \mathbf{A}\mathbf{A}^T, \quad (9)$$

where  $\hat{\vec{x}}(k|l) = \mathcal{E}\{\vec{x}(k)|\vec{z}(1) \dots \vec{z}(l)\}$  and  $\mathbf{P}(k|l) = \mathcal{E}\{(\vec{x}(k) - \hat{\vec{x}}(k|l))(\vec{x}(k) - \hat{\vec{x}}(k|l))^T | \vec{z}(1) \dots \vec{z}(l)\}$ . Decentralized EKF implements the prediction equation over all nodes.

For the filtering stage, each active node converts its measurements into information for the target state and covariance updates,

$$y_i(k+1) = \frac{1}{\sigma_i^2} \nabla_i \left[ z_i(k+1) - H_i \left( \hat{x}(k+1|k) \right) + \nabla_i^T \hat{x}(k+1|k+1) \right],$$

$$\mathbf{Y}_i(k+1) = \frac{1}{\sigma_i^2} \nabla_i \nabla_i^T,$$

where  $\nabla_i$  is the gradient of  $h_i(\vec{x})$  about  $\hat{x}(k+1|k)$ . It can be shown that

$$\nabla_i = \frac{1}{r_i} (-\sin(\phi_i), \cos(\phi_i), 0, 0)^T.$$

The active nodes communicate their information,  $y_i$  and  $\mathbf{Y}_i$ , with the other nodes. The nodes then implement the filter equations,

$$\hat{x}(k+1|k+1) = \mathbf{P}_i(k+1|k+1) \left( \mathbf{P}_i^{-1}(k+1|k) \hat{x}(k+1|k) + \sum_{i \in \mathcal{N}_a} y_i(k+1) \right), \quad (10)$$

$$\mathbf{P}^{-1}(k+1|k+1) = \mathbf{P}^{-1}(k+1|k) + \sum_{i \in \mathcal{N}_a} \mathbf{Y}_i(k+1) \quad (11)$$

It can be shown that the inverse covariance update in (11), i.e.,  $\sum \mathbf{Y}_i$ , is equivalent to the FIM in (7).

### 3.3 Initialization

The issues dealing with target detection, track initiation and multi-target data association are beyond the scope of this paper. We assume that all nodes are able to detect the target and estimate the DOA, albeit a possible poor estimate due to (4). In our simulations, the track is initiated by using the TS-WNLS (see (5)) over the first two snapshots using all  $N_s$  nodes in the network. The localization provides estimates of the target position  $\hat{p}(1)$  and  $\hat{p}(2)$  and velocity  $\hat{v}(2) = (\hat{p}(2) - \hat{p}(1))/T$ . Then,  $\hat{x}(2) = [\hat{p}(2)^T \hat{v}(2)^T]^T$  and

$$\mathbf{P}(2|2) = \begin{pmatrix} \mathbf{J}^{-1}(2) & \mathbf{J}^{-1}(2) \\ \mathbf{J}^{-1}(2) & \frac{1}{T^2}(\mathbf{J}^{-1}(1) + \mathbf{J}^{-1}(2)) + \sigma_v^2 \mathbf{I} \end{pmatrix},$$

where  $\mathbf{J}$  is the FIM for the first and second snapshots.

## 4 ACCURACY BOUNDS FOR LOCALIZATION

As documented in the previous section, the FIM given by (7) indicates the localization accuracy of the active nodes. For single snapshot localization, the covariance matrix for the position estimate is the inverse of the FIM, and the RMS error is given by (6). For target tracking, the FIM is added to the inverse of the predicted covariance to form the inverse of the filtered covariance (see (11)). The covariance

update equation suggest that the norm of the FIM should be large so that the trace of  $\mathbf{P}(k|k)$ , or equivalently, the RMS position error, becomes as small as possible. Therefore, it is sensible to minimize (6) to select nodes with good localization geometries for both single snapshot and tracking implementations.

This section analysis the structure of (6) to develop heuristical claims about the best node/target geometries. Given two bearing sensors, it is well known that in order to achieve accurate position estimates, it is desirable for line of sights between the nodes and the target to be orthogonal. In addition, if the bearing error is fixed, it is better for the nodes to be closer to the target. Interesting (6) can be bounded by the ‘‘effective average’’ distance from the active nodes to the target as given by the following theorem.

**Theorem 1** *The RMS position error for an active sets of nodes  $\mathcal{N}_a$  given by (6) is bounded below by*

$$\rho \geq \frac{2M_{r\sigma}}{\sqrt{N_s}} \quad (12)$$

where

$$M_{r\sigma} = \left( \frac{1}{N_s} \sum_{i \in \mathcal{N}_a} \frac{1}{\sigma_i^2 r_i^2} \right)^{-\frac{1}{2}}. \quad (13)$$

*Proof:* By inspection of (7), it is clear that the  $2 \times 2$  FIM is positive semi-definite, and  $\text{trace}\{\mathbf{J}\} = \frac{N_s}{M_{r\sigma}^2}$ . Therefore, the two eigenvalues of  $\mathbf{J}$  can be represented as

$$\lambda_2^{\max} = \frac{1}{2} \frac{N_s}{M_{r\sigma}^2} (1+a), \quad \lambda_2^{\min} = \frac{1}{2} \frac{N_s}{M_{r\sigma}^2} (1-a),$$

where  $0 \leq a \leq 1$ . Furthermore,

$$\begin{aligned} \text{trace}\{\mathbf{J}^{-1}\} &= \frac{1}{\lambda_2^{\max}} + \frac{1}{\lambda_2^{\min}} \\ &= \frac{\lambda_2^{\max} + \lambda_2^{\min}}{\lambda_2^{\max} \lambda_2^{\min}} \\ &= \frac{\text{trace}\{\mathbf{J}\}}{\det\{\mathbf{J}\}}. \end{aligned} \quad (14)$$

Because,

$$\begin{aligned} \det\{\mathbf{J}\} &= \frac{1}{4} \left( \frac{N_s}{M_{r\sigma}^2} \right)^2 (1-a^2), \\ &\leq \frac{1}{4} \left( \frac{N_s}{M_{r\sigma}^2} \right)^2, \end{aligned}$$

then

$$\text{trace}\{\mathbf{J}^{-1}\} \geq \frac{4M_{r\sigma}^2}{N_s}.$$

By taking the square root of both sides, the bound in (12) follows. **Q.E.D.**

The theorem shows that the lower bound for the RMS error is proportional to the ‘‘average’’ range of the nodes to

## 5 GLOBAL NODE SELECTION

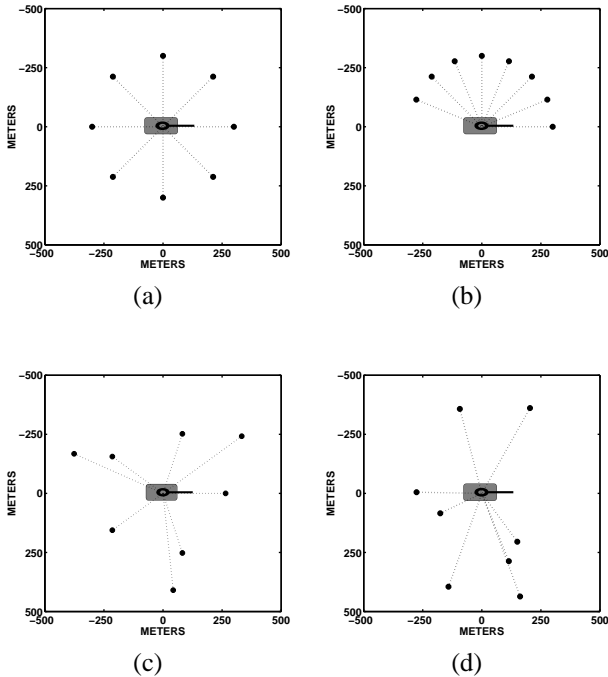


Figure 3: RMS error bound achieving sensor network configurations consisting of 8 nodes where the “average” target range is 300 meters: (a) One 360° ring, (b) one 180° ring, (c) two 360° rings and (d) random.

the target. Specifically,  $M_{r\sigma}$  is the reciprocal root mean reciprocal effective range squared. Clearly, it is desirable for the nodes to be close to the target and provide good bearing estimates in order to accurately localize the target. In fact, the bound given by (12) indicates that the bearing error and range to the target have equal effects on the lower bound of the RMS position error, where the effective range to the target is  $r_{\sigma,i} = \sigma_i r_i$  for the  $i$ -th node.

When the bearing error model in (4) is isotropic, a sufficient, but not necessary, condition to achieve the bound in Theorem 1 is that the active nodes are uniformly spaced along concentric semi-circular or circular rings surrounding the target (Kaplan 2002). Figure 3 shows examples of node configurations that meet the bound where  $N_a = 8$ . Figures 3a-c are examples of the concentric rings, and Figure 3d was generated by randomly placing seven sensors and inserting the eighth sensor in one of two spots on the ground so that the bound can be achieved. These bound achieving configurations indicate that the active nodes must surround the target. Therefore, the best active nodes for TS target localization are the ones that are effectively close to the target in the  $r_{\sigma,i}$  sense and provide diverse angular views of the target.

Analytically, a node selection algorithm selects an active subset of nodes to minimize the root mean squared (RMS) position error of the target under the low power constraint. Because power usage is directly correlated to the number of active sensors, it is reasonable to constrain the number of active nodes. Otherwise, one would simply localize the target with all nodes. Previous algorithms for node selection appear in (Zhao et al. 2002) for range sensor nodes and in (Kadar 1998) for the selection of a small number, i.e.,  $N_a = 3$ , of active bearing nodes.

This section describes two global node selection techniques that were analyzed in (Kaplan 2002). These techniques can select an arbitrary number or active nodes. They are global in the sense that they consider the location of **all**  $N_s$  network nodes relative to the target position, i.e.,  $(r_i, \phi_i)$  in (7), to determine the active set  $\mathcal{N}_a$ . The algorithms are designed with the intention that (6) will be small for a set  $\mathcal{N}_a$  containing  $N_a$  nodes. To this end, we assume that the absolute node positions are known. In practice, the wireless sensor network will self-calibrate to generate absolute position estimates of the nodes (Moses et al. 2001; Cevher and McClellan 2001). While the network is tracking a target, the node selection approach will use the predicted target location  $\hat{x}(k+1)$  to determine the relative positions of the nodes. The two node selection methods are described below.

**Closest Sensors:** The “closest” sensors approach simply chooses the  $N_a$  sensors with the smallest range to the target. This approach is computationally simple, and it is sensible because for isotropic bearing error models (see (4)), the lower bound in (12) is as small as possible. The drawback of the approach is that it does not consider the angular diversity of the sensors. In addition, it does not consider the bearing measurement error  $\sigma_i$  at each node.

**Simplex:** The simplex method is a greedy approach and requires knowledge of the quality of the DOA estimates, i.e.,  $\sigma_i$ , as well as an estimate of the target position from the tracker. Note that  $\sigma_i$  can be extracted from SNR estimates (Bethel and Bell 2002). Using  $\hat{x}(k+1|k)$  and  $\hat{\sigma}_i$  for  $i = 1, \dots, N_s$ , the simplex is initialized by selecting the optimal active subset of two nodes that minimizes (6). Then, one node is added at a time to minimize (6) until the active subset contains  $N_a$  nodes. The simplex method then attempts to improve this initial selection of nodes by checking to see if replacing a node in the active set with an inactive node improves the localization accuracy. Specifically, the nodes in the initial active set are arranged into slots in the order they were added to the active pool by the add one at a time initialization. The simplex starts at the  $N_a - 1$  slot and checks to see if exchanging the node in that slot with a node outside the active pool improves the overall RMS error. If no improvement is possible, then the next smaller slot is checked. Otherwise, the better node goes

into the slot, the replaced node goes into the inactive pool and slot  $N_a$  is checked. For any slot that is checked, if no nodes outside the active set improves the RMS error, then the next smaller slot is checked. Otherwise, the better node replaces the node in the slot and slot  $N_a$  is checked. Once the first slot is checked, and no node improves the RMS error, then the algorithm terminates. The simplex is guaranteed to converge because the number of possible configuration is finite. Typically, the convergence require only a few iterations.

In (Kaplan 2002), these algorithms were compared to more computationally expensive optimal selection algorithms. Empirical results over 1000 random configuration of nodes demonstrate that the simplex is nearly optimal and the closest approach increased the RMS position error about 14% for the isotropic propagation model in (4) with  $\alpha = 1$ . Clearly, the simplex approach can determine which  $N_a$  nodes provide a good geometry for geolocation.

Because the closest and simplex methods consider the location of all nodes, they are not scalable as more nodes are added to the network. In other words, it is not possible to distribute these algorithms over the nodes so that the computational complexity per node remains constant as the size of the sensor network increases. Either the algorithms must be implemented on a centralized processor or implemented over all nodes. The first option option is not possible for a robust and self-healing network. The second option wastes computational resources.

## 6 AUTONOMOUS NODE SELECTION

The main result of this work is an autonomous node selection algorithm that does not require global knowledge of the network. Using the autonomous approach, each node independently determines whether or not to participate as an active sensing node for the upcoming snapshot using only knowledge of the location of the active nodes from the previous snapshot. We refer to this approach as the *autonomous nodes selection* (ANS) algorithm. The ANS algorithm works by each node evaluating its ability to increase the **utility** of the active set of nodes. Specifically, the *utility* of a set of nodes is inversely proportional to resulting RMS position error in (6) via

$$\mu = \frac{1}{\rho^2}.$$

Note that the utility is a function of the active set of nodes  $\mathcal{N}_a$ , and the goal is to find the  $\mathcal{N}_a$  of small cardinality that maximizes the utility. If node  $i$  was active during the previous snapshot, the differential utility for keeping the node active is

$$d\mu(i|\mathcal{N}_a) = \mu(\mathcal{N}_a) - \mu(\mathcal{N}_a \setminus \{i\}). \quad (15)$$

The nodes decides to remain active if and only its differential utility is one of  $N_d$  largest for the active set of nodes

from the previous snapshot. Note that  $N_d$  is a user defined parameter that determines the minimum number of nodes active per snapshot. Otherwise, if node  $i$  was inactive, the differential utility for node to become active is

$$d\mu(i|\mathcal{N}_a) = \max_{a \in \mathcal{N}_a} \mu(\mathcal{N}_a \setminus \{a\} \cup \{i\}) - \mu(\mathcal{N}_a \setminus \{a\}). \quad (16)$$

If this  $d\mu$  exceeds a threshold, then the node becomes active for the next snapshot. The threshold is set during the previous snapshot as the  $\kappa$ -th largest value of  $d\mu$  of the active nodes, where  $\kappa$  is a parameter that controls the flexibility of the algorithm to allow inactive nodes to join the active set. Clearly, both the  $N_d$  and  $\kappa$  parameters provide a mechanism to trade-off localization accuracy against power, i.e., node usage.

The ANS algorithm only needs to consider the bearing errors  $\sigma_i$  and relative locations  $(r_i, \phi_i)$  of the active nodes and itself to determine whether or not to actively sense and communicate for the next snapshot. This information is naturally communicated between nodes during tracking for the covariance filter update (see (11) and (6)). Because a node only needs collaboration from the active set of nodes using information used in the EKF, the ANS algorithms fits naturally into the decentralized Kalman filter framework (Rao and Durrant-Whyte 1991). The dominant complexity of (15) and (16) is the calculation of the FIM using (7), which is  $O(N_a)$ . Therefore, ANS is  $O(N_a)$ . Clearly, the size of the network  $N_s$  does not effect the complexity of the ANS method. Therefore, the ANS is scalable. In contrast, the simplex methods is  $O(N_s^2)$ . The complexity of the simplex is dominated by its initialization process of finding the two nodes in the network that minimizes (6). To avoid central node management processor and to reduce communication requirements, the simplex can be reproduced on every node. As the size of the network becomes large, it is clear that the computational complexity of the simplex grows without bound.

## 7 EXPERIMENTAL RESULTS

We compared the sensor selection algorithms through simulation of a constant velocity target traveling through a wireless sensor network. The simulations use (1)-(3) to model the bearing measurements. The network consists of  $N_s = 50$  nodes randomly placed in a 1km  $\times$  2km region. Figure 4 shows the active nodes during different stages of target tracking when implementing the ANS using  $N_d = 5$  with a high ( $\kappa = 1$ ) and low ( $\kappa = 5$ ) threshold setting in the left and right column, respectively. The target is moving horizontally at a speed of 10m/s and the snapshot interval is  $T = 1$  seconds. The bearing errors follows the anisotropic model with  $\alpha = 0$ , and the EKFs were run using an accelerating standard deviation  $\sigma_v = 1\text{m/s}^2$ . The rows in Figure 4 represent different snapshots. At the earlier snapshot, the localization is poor. As more measurements are integrated

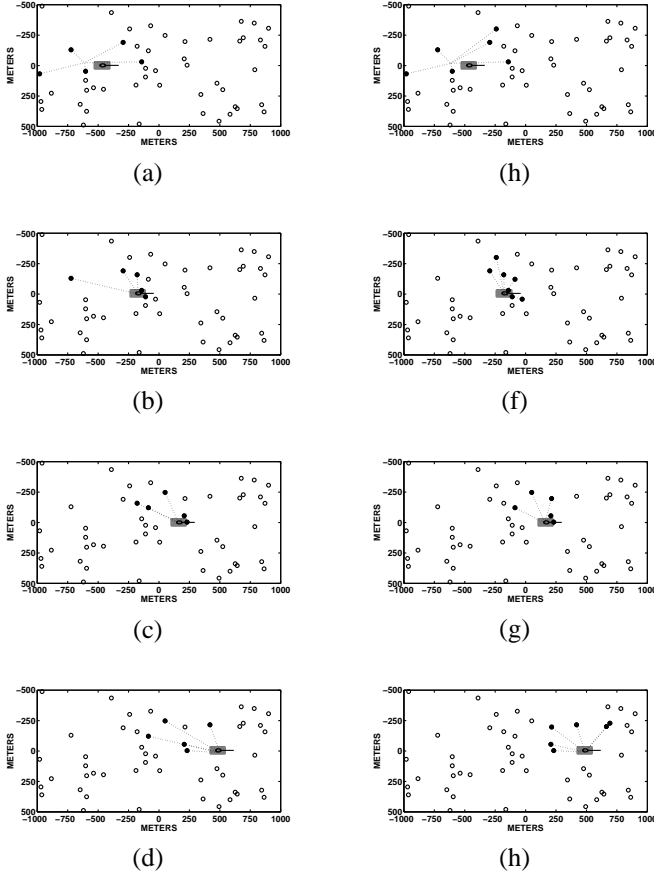


Figure 4: ANS results during decentralized EFK tracking with  $N_d = 5$  for different snapshots: (a)-(d):  $\kappa = 1$  and (e)-(h):  $\kappa = 5$ .

over more snapshots, the EKF is able to better localize the target. The figure shows that the higher threshold leads to less active nodes per snapshot, because it is less likely for inactive node to decide to activate for the next snapshot. As a results, the active nodes tend to be further from the target than for the low threshold setting. By considering (12), the localization performance at the lower threshold is better at the cost of more sensors per snapshot.

We ran 100 Monte Carlo simulations of a 10m/s target traveling through the sensor field in Figure 4 for the different selection algorithms. Figure 5 compares the node usage and RMS position error for the autonomous algorithm as a function of  $\kappa$  when  $N_d = 5$ . The figure includes results for different bearing error models (see Figure 2): 1) isotropic with  $\alpha = 0$ , 2) isotropic with  $\alpha = 1$  and 3) anisotropic with  $\alpha = 0$ . Note that the EKF was not able to converge for the anisotropic model with  $\alpha = 1$  because the bearing measurements are so poor. The results in Figure 5 were obtained by setting  $\sigma_\nu = 0\text{m/s}^2$  in the EKF. It turns out that one random tracking realization did not converge for the anisotropic model with  $\alpha = 0$  when implementing the simplex selection method. Furthermore, four

realizations did not converge for the isotropic model with  $\alpha = 1$  when using one or more of the different node selection algorithms. These outlier realizations were purged when computing the average results illustrated in Figure 5. The figure also includes results for the global approaches, i.e., closest and simplex, as horizontal lines with  $N_a = 6$ . The figure demonstrates the tradeoff between localization performance and node usage. For equivalent node usage, the ANS algorithm achieves nearly as good localization performance as the simplex for all bearing error models. In fact, the ANS algorithm outperforms the simplex when  $\alpha = 1$  for the isotropic case. Clearly, the ANS algorithm shows promise as a means to maintain good localization performance while conserving energy.

It is interesting to note that the simplex algorithm always outperform the closest algorithm. However, the relative increase in RMS position error of the closest approach as compared to the simplex is only about 5% for the isotropic bearing error models. In contrast, the relative increase is over 25% for the nonisotropic case. For the isotropic model, when the closest sensors do provide a poor geometry for a particular snapshot, e.g., collinear nodes and target, the viewing geometry can become very good after a couple of snapshots due to the movement of the target. Therefore, these poor viewing geometries are averaged out by the EKF. In contrast, the sensors below the target provide very poor measurements for the anisotropic case, and the closest nodes will continue to provide poor viewing geometries for a number of snapshots.

We also investigated results for other values of  $\sigma_\nu$  and the mean results are similar. Interesting, as the flexibility to track maneuvering targets increases by increasing  $\sigma_\nu$  from zero, the number of divergent realizations decreases. For example, when  $\sigma_\nu = 5\text{m/s}^2$ , all 100 realizations converge for all three bearing error models. This result is due to the fact that the EKF can forget poor initial measurements better as  $\sigma_\nu$  increases from zero. However, we also observed that as  $\sigma_\nu$  goes to infinity, the EKF no longer converges because it is too dependent on measurements from the present snapshot.

## 8 CONCLUSIONS AND FUTURE DIRECTIONS

This paper introduced and analyzed a new decentralized node selection algorithm, autonomous node selection, for wireless sensor networks. Simulations show that the ability for ANS to select nodes with good localization geometries is comparable to the global simplex algorithm. In fact, the simulations shows that selecting the closest nodes to the predicted target location provides only slightly worse performance than the simplex method for an isotropic bearing error model. For anisotropic model, the closest nodes approach is significantly worse than the simplex. Interestingly, the effective range  $r_{i,\sigma}$  is proportional to the true

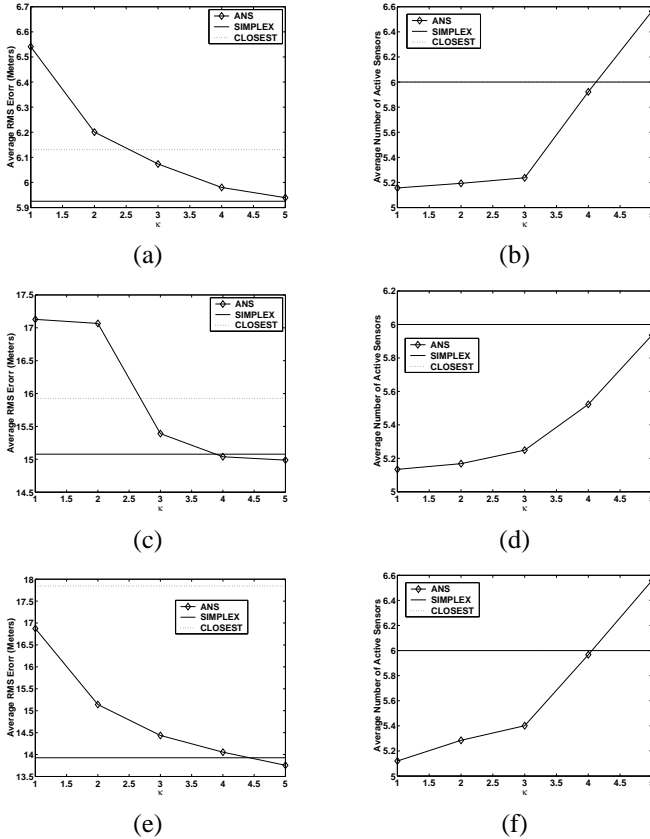


Figure 5: Comparison of node selection algorithms for varying bearing error models: (a)-(b) isotropic with  $\alpha = 0$ , (c)-(d) isotropic with  $\alpha = 1$  and (e)-(f) anisotropic with  $\alpha = 0$ . The plots show two different performance measures: (a),(c),(e) Average RMS position error and (b),(d),(f) average number of active nodes per snapshot.

range  $r_i$  for the isotropic model and the closest approach can decrease the lower bound in (12). To lower this bound for the anisotropic model, one can choose the closest nodes in the sense of  $r_{i,\sigma}$ . Initial tests shows that this approach provides similar performance to the simplex for both general bearing error models. A decentralized version of the effective closest node selection approach can lead to computationally simpler expressions for differential utility than the ANS. We plan to evaluate the performance of such a decentralized selection algorithm in the near future. In addition, we plan to evaluate the node selection approaches while tracking a maneuvering target.

Future work will investigate multi-target tracking issues for node selection such as localization accuracy, data association and track initiation. Furthermore, we plan to extend the utility function to consider the battery level and the radiation power needed for communication. At the present time, we assume that each node broadcasts information to all the other nodes in the network. Because the active nodes should form clusters around each target, the communica-

tion range can be reduced. In the end, we hope to develop a joint communication and sensing protocol for tracking targets in a wireless sensor network.

## References

- Bethel, R. E. and K. L. Bell: 2002, A MLE approach to joint source detection and direction of arrival estimation. *Proc. of IEEE SAM*, Rosslyn, VA.
- Cevher, V. and J. H. McClellan: 2001, Sensor array calibration via tracking with the extended Kalman filter. *Proc. of the 2001 ARL Federated Laboratory Symposium*, College Park, MD, 51–55.
- Kadar, I.: 1998, Optimum geometry selection for sensor fusion. *Proc. of SPIE*, volume 3374, 96–107.
- Kaplan, L. M.: 2002, Node selection for target localization in a distributed network of bearings-only sensors, to be submitted to *IEEE Trans. on Aerospace and Electronic Systems*.
- Kaplan, L. M. and Q. Le: 2002, Analysis of target localization methods using bearings-only measurements for wireless sensor networks, to be submitted to *IEEE Trans. Signal Processing*.
- Kaplan, L. M., Q. Le, and P. Molnar: 2001a, Fusion of bearing measurements from acoustical unattended ground sensors for target localization. *Proc. of the 2001 ARL Federated Laboratory Symposium*, College Park, MD, 39–44.
- Kaplan, L. M., P. Molnar, and Q. Le: 2001b, Bearings-only target localization for an acoustical unattended ground sensor network. *Proc. of SPIE*, volume 4393, 40–51.
- Magill, B. and D. Swanson: 1999, Modeling outdoor sound propagation with modeled weather data. *Proc. of IRIS Acoustic and Seismic Sensing*, volume 1, 241–246.
- Moses, R., R. Patterson, D. Krishnamurthy, N. Srour, and T. Pham: 2001, Self-calibration of unattended ground sensor networks. *Proc. of the 2001 ARL Federated Laboratory Symposium*, College Park, MD, 63–68.
- Nardone, S., A. G. Lindgren, and K. F. Gong: 1984, Fundamental properties and performance of conventional bearings-only target motion analysis. *IEEE Trans. on Automatic Control*, **29**, 775–787.
- Peach, N.: 1995, Bearings-only tracking using a set of range-parameterised extended Kalman filter. *IEEE Proc. of Control Theory Appl.*, **142**, 73–80.
- Rao, B. S. and H. F. Durrant-Whyte: 1991, Fully decentralized algorithm for multisensor Kalman filtering. *IEE Proceedings-D*, **138**, 413–420.
- Zhao, F., J. Shin, and J. Reich: 2002, Information-driven dynamic sensor collaboration. *IEEE Signal Processing Magazine*, **19**, 61–72.

The views and conclusions contained in this document are those of the authors and should not be interpreted as presenting the official policies either express or implied of the Army Research Laboratory or the U. S. Government.